THE ASTROPHYSICAL JOURNAL, 177:723–743, 1972 November 1

MASSES AND RADII OF WHITE DWARFS

H. L. SHIPMAN*
Hale Observatories, California Institute of Technology, Carnegie Institution of Washington
Received 1972 May 12

ABSTRACT

Additional model atmospheres representing the surface layers of hydrogen-rich and helium-rich white dwarfs have been calculated and are presented in tables. These model atmospheres and multichannel photoelectric scans by Oke have been used to determine the masses of 19 and the radii of 26 stars in Oke's observing program. The median radius of the program stars, which are in general among the intrinsically brightest white dwarfs, is 0.013 $R_\odot$, and the median mass is 0.52 $M_\odot$. The DA stars have effective temperatures between 6000° and 50,000° K, with $N(\mathrm{He}) < 0.008$ by number. The DB stars have $12{,}000° \leq T_{\mathrm{eff}} \leq 18{,}000°$ K, and calcium abundances $\lesssim 0.01$ of the solar value.

The program stars are then used to calibrate a $U - V$ versus T_{eff} relation, and radii are determined for all white dwarfs with known distances. The median radius of this sample of stars, which contains more intrinsically faint stars than the set of program stars, is 0.0095 $R_\odot$. The masses of some of these stars are found from surface gravities derived from the m_1-indices of Graham. The masses and radii found here are in satisfactory agreement with the mass-radius relation for degenerate stars and with measured gravitational redshifts.

The above analyses were applied for the purpose of testing the convection-accretion hypothesis of Strittmatter and Wickramasinghe, which purports to explain the existence of the DB stars. The present results contradict their prediction that there should be a shortage of DA stars with effective temperatures between 15,000° and 18,000° K. I propose a modification of their hypothesis which explains the existence of DB and DC stars in the observed temperature ranges.

I. INTRODUCTION

White dwarfs are luminous objects of solar masses and planetary dimensions. The determination of accurate values for the mass and radius of these objects is a difficult matter, and has been done for only a few stars. Masses have been computed for three stars—Sirius B, Procyon B, and 40 Eri B—by analysis of binary star orbits, and the radius of 40 Eri B can be evaluated by means of the accurate gravitational-redshift measurement of Popper (1954). Other determinations of the masses of white dwarfs rest on more shaky theoretical grounds. The measurements of gravitational redshifts by Greenstein and Trimble (1967) only provide values for the ratio M/R, and computation of the mass and radius requires a temperature scale. The temperature scales hitherto proposed are not very reliable. Previous attempts at model-atmosphere analyses of white dwarfs (Terashita and Matsushima 1969; Matsushima and Terashita 1969*a*, *b* [hereafter these three papers are collectively referred to as TM]; see also Bues 1970, Strittmatter and Wickramasinghe 1971) have encountered difficulties in transforming model-atmosphere flux distributions to *UBV* colors, since the observational basis for their analyses was the *UBV* system.

In this paper, I shall use multichannel observations by Oke (1972), together with appropriate model atmospheres, to calculate masses and radii of white dwarfs. The multichannel observations represent the energy distribution of the star over a wide wavelength range, and one can compare model-atmosphere results with observations without using transformation formulae, which are not accurately known. In § II

* Present address: Yale University Observatory.

I describe the model atmospheres used in this study, and in §§ III–VIII I discuss the analysis of white dwarfs from multichannel observations for different types of stars, proceeding from the most reliable analyses to the most unreliable. In §§ IX and X, I use the results from the preceding sections to calibrate the *UBV* and *ubvy* observations, and I then determine masses and radii for a larger sample of stars. In § XI the model-atmosphere results are compared with the gravitational-redshift measurements, and in §§ XII and XIII the results of this study are applied to theories of the structure and evolution of white dwarfs.

II. MODEL ATMOSPHERES

The model atmospheres presented here were calculated with the program ATLAS (cf. Kurucz 1969*a*, *b*). Opacity sources included in all models were H, He, C, N, O, Ne, Mg, and Si in appropriate stages of ionization, He^-, H^-, electron and Rayleigh scattering. The He^- opacity subroutine was that of Gingerich *et al.* (1966); all other opacity subroutines are described by Kurucz (1969*b*). The temperature range covered by the hydrogen-rich models, which had H = 0.9 and He = 0.1 by number and a solar metal abundance, is $6000° \leq T_{\rm eff} \leq 50{,}000°$ K. The models for DB (helium-rich) white dwarfs have $6000° \leq T_{\rm eff} \leq 22{,}000°$ K with $\log g = 8$ and $T_{\rm eff} = 14{,}000°$ and 17,000° for $\log g = 7$. The composition of the DB models is He = 1, H = 0, and two values for the metals/(total number of atoms) ratio: the solar value and zero. The zero-metal models for $T_{\rm eff} = 10{,}000°$ and 6000° K were omitted. The solar mixture of metals was the standard one (Goldberg, Müller, and Aller [GMA] 1960). Convection was neglected in all of the DA models, but was included in the DB models. A full description of the calculation procedures can be found in Shipman (1971*a*); the following paragraphs present the highlights of the model results. In addition, I will supply such desiderata as temperature structures on request.

The models for DA stars with $T_{\rm eff} \geq 12{,}000°$ K have been presented elsewhere (Shipman 1971*b*). Calculation of the cooler models presented here followed the same procedures used in the calculation of the hotter models presented earlier: line blanketing was included and convection was neglected. Although the models with $8000° \leq T_{\rm eff} \leq 12{,}000°$ K were convectively unstable, the uncertainties of fitting models to observations in this temperature range would render the inclusion of convection somewhat unproductive. The Griem (1964) line-broadening theory was used in the hydrogen-line calculations; at white-dwarf densities this theory is virtually identical to the Edmonds, Schlüter, and Wells (1967) semiempirical theory. Iteration was terminated when flux errors were a few tenths of a percent.

Emergent fluxes for selected wavelengths and data for the Hγ line are presented in table 1, for the models not published previously. The parameter $D(0.2)$ is the full width of the line where the line depth is 0.2. Emergent fluxes H_ν are normalized so that $\int H_\nu d\nu = \sigma T_{\rm eff}^4/(4\pi \times 10^4)$. The notation under "Model" corresponds, as before, to [$T_{\rm eff}/10^3$, $\log g$; metals/GMA, N(He)/(total number of atoms)]. GMA refers to the solar abundances mentioned above, and the metal abundance is given in terms of the ratio N(metals)/(total number of atoms).

The principal theoretical result from the additional DA models is that the hydrogen lines weaken extremely rapidly with decreasing effective temperature for $T_{\rm eff} \leq 10{,}000°$ K. This weakening is caused by the abrupt onset of H^- absorption at these temperatures. As explained by Weidemann (1963), white dwarfs with $T_{\rm eff} \lesssim 8000°$ K will have hydrogen lines about as strong as hydrogen lines in main-sequence stars of the same temperature ($\sim$10–15 Å in equivalent width). This value is a sharp drop from an equivalent width of 42 Å at $T_{\rm eff} = 12{,}000°$ K, $\log g = 8$. In general, the DA models are quite reliable, as the relevant physics, such as the value for the absorption coefficient of hydrogen, is well known.

TABLE 1 - DA MODEL DATA

Model	6,7; 1,0.1	8,7; 1,0.1	10,7; 1,0.1	6,8; 1,0.1	8,8; 1,0.1	10,8; 1,0.1
λ(Å)	Emergent Fluxes					
3122	.026	.104	.229	.026	.113	.268
3364	.030	.114	.239	.031	.123	.278
3647	.036	.125	.249	.036	.134	.287
4058	.045	.175	.422	.044	.164	.384
4102	.033	.072	.160	.037	.076	.165
4148	.047	.179	.431	.046	.168	.393
4219	.048	.187	.488	.047	.175	.445
4292	.049	.183	.434	.048	.172	.399
4340	.037	.081	.173	.039	.078	.175
4393	.051	.186	.438	.050	.175	.465
4521	.053	.194	.498	.052	.182	.459
4656	.055	.196	.488	.054	.184	.406
4800	.057	.193	.431	.056	.182	.330
4861	.048	.100	.197	.047	.094	.197
4927	.059	.195	.430	.058	.184	.443
5242	.064	.202	.460	.063	.191	.426
5600	.068	.203	.439	.067	.192	.407
6010	.072	.202	.415	.071	.192	.361
6485	.076	.198	.370	.075	.189	.314
6563	.069	.128	.220	.068	.124	.222
6646	.077	.198	.364	.076	.188	.359
7611	.082	.191	.337	.081	.184	.295
8206-	.083	.185	.312	.082	.178	.331
8206+	.083	.187	.342	.082	.179	.295
10504	.084	.162	.257	.083	.156	.212
Δλ	H_γ RESIDUAL INTENSITIES					
0.0	.385	.335	.289	.401	.355	.317
1.0	.698	.413	.353	.713	.427	.387
3.0	.862	.562	.412	.862	.579	.445
5.0	.918	.654	.459	.917	.673	.487
10.0	.968	.779	.557	.966	.796	.582
20.0	.990	.885	.697	.990	.897	.719
30.0	.996	.932	.788	.996	.941	.804
40.0	.998	.958	.851	.998	.964	.861
50.0	.999	.973	.896	.999	.977	.903
60.0	1.000	.983	.930	.999	.985	.933
80.0	1.000	.994	.974	1.000	.995	.974
100.0	1.000	1.000	1.000	1.000	1.000	1.000
D(0.2)	3.9	22.0	63.4	3.7	20.6	62.6
W(Å)	3.2	15.4	33.5	3.0	14.1	31.5

The DB models are considerably more difficult to calculate than the DA models, principally because of the problems of convection. The convection theory used here was a variation of the mixing-length theory proposed by Böhm and Stückl (1967), which takes into account the fact that the geometrical height from, say, $\tau = 50$ to the top of the convective layer is considerably less than one scale height. Thus the effective mixing length, or the mean free path of a convective blob, is about 0.3 times the pressure scale height. The convective flux is less than the flux computed by traditional methods (e.g., setting the mixing length equal to the pressure scale height) by a factor of about 9. In a refinement of the Böhm-Stückl theory, the integrals of motion of the convective blobs were evaluated numerically, rather than being estimated from the local value of the temperature gradient. A fuller description of this procedure is given elsewhere (Shipman 1971*a*).

The value of the convective flux computed by the present procedure is still quite crude, for numerous complications have been ignored. Viscous forces and convective overshoot have been neglected. The high densities of DB atmospheres lead to convective velocities which are appreciable fractions of the sonic velocity, and the

problems of supersonic convective motions would have to be considered in any thorough treatment. A most serious complication is that the convective blobs will lose energy radiatively as they rise, while the mixing-length theory assumes that a blob rises adiabatically.

Improving the convection theory along these lines would, in general, reduce the convective efficiency, and cause the real star to behave more like a radiative model. If the convective efficiency were zero and if real stars were completely radiative, the effective temperatures of DB stars deduced in this paper would be too high by 1000°–2000° K, according to the calculations of Wickramasinghe and Strittmatter (1971). This change is comparable to the uncertainties which arise from the procedure of fitting models to real stars.

The DB models also suffer from an uncertainty of about 15 percent in the value of the He^- absorption coefficient, which is the dominant one in these atmospheres. Because of this problem, in addition to the problems with convection, adherence to the usual model-atmosphere criterion of a few tenths of a percent for flux constancy is unnecessary. Such flux constancy is meaningless when uncertainties in the physical theory lead to uncertainties in the total flux of 20–30 percent; consequently iteration of the models was terminated when flux errors were a few percent. Flux errors somewhat greater than this were tolerated in two cases: at the top two depth points of the convective layer, where the total flux was extremely sensitive to very small ($\lesssim 100°$ K) changes in temperature, and at the bottom two depth points of the atmosphere. These models should be regarded as very tentative; more accurate model atmospheres for DB stars must wait until the problems with the theory of convection are worked out and the He^- absorption coefficient is evaluated more accurately. The broadening theory of Barnard, Cooper, and Shamey (1969) was used for He I λ4471.

Emergent fluxes and the equivalent width of He I λ4471, $W(4471)$, are presented for the DB models in tables 2 and 3. In computing $W(4471)$ the continuum was arbitrarily set by letting the residual intensity be 1.000 at a point 150 Å from line center. The notation and normalization of the fluxes is the same as that in table 1.

Models representative of DB stars have been previously calculated by Bues (1970) and by Strittmatter and Wickramasinghe (1971; hereafter SW). Bues did not include the effects of convection, and consequently the temperatures at points within the convective zone are higher in her models than in the present models. Therefore, at a given effective temperature, the emergent fluxes from her models are indicative of a higher temperature, and her values of $W(4471)$ are greater than mine. SW included

TABLE 2 - DB MODELS

Model	14,7 0,1	17,7 0,1	14,8 0,1	17,8 0,1	22,8 0,1	6,8 1,1
λ(Å)	Emergent Fluxes					
3122-	1.04	1.44	.96	1.57	2.71	.049
3122+	1.04	1.46	.96	1.59	2.76	.049
3265	1.04	1.43	.97	1.56	2.64	.052
3422-	1.03	1.40	.97	1.52	2.52	.054
3422+	1.10	1.71	1.00	1.73	3.19	.054
3530	1.10	1.67	1.00	1.69	3.08	.055
3680-	1.08	1.61	.99	1.64	2.94	.057
3680+	1.10	1.72	1.00	1.70	3.17	.057
4038	1.05	1.59	.97	1.57	2.85	.061
4472	.98	1.43	.93	1.43	2.50	.062
5011	.90	1.26	.86	1.27	2.14	.064
5699	.79	1.08	.78	1.10	1.77	.063
6726	.66	.88	.66	.89	1.37	.058
8206	.51	.67	.52	.68	1.00	.051
10504	.36	.46	.37	.46	.67	.042
W(4471)	6.71	14.70	5.01	13.12	24.78	0

TABLE 3 - DB MODELS

Model	10,8 1,1	14,7 1,1	17,7 1,1	14,8 1,1	17,8 1,1	22,8 1,1
λ(Å)	Emergent Fluxes					
3122-	.40	1.20	1.83	1.24	1.89	3.12
3122+	.40	1.21	1.85	1.25	1.92	3.17
3265	.40	1.20	1.81	1.24	1.87	3.03
3422-	.41	1.18	1.77	1.22	1.81	2.93
3422+	.41	1.31	2.16	1.30	2.18	3.55
3530	.41	1.29	2.10	1.27	2.12	3.43
3680-	.41	1.26	2.03	1.25	2.04	3.28
3680+	.41	1.30	2.20	1.26	2.16	3.52
4038	.41	1.22	1.91	1.18	1.97	3.15
4472	.40	1.13	1.80	1.16	1.76	2.76
5011	.40	1.02	1.58	.99	1.54	2.36
5655	.38	.90	1.35	.87	1.31	1.96
6726	.34	.74	1.08	.72	1.05	1.52
8206	.28	.57	.82	.58	.79	1.12
10504	.21	.40	.55	.39	.54	.75
W(4471)	1.08	9.16	15.3	8.82	18.11	17.84

convection, but used the classical mixing-length theory without the Böhm-Stückl modifications described above. Although precise comparison is difficult because SW used a different grid of metal abundances, the values of $W(4471)$ computed by them and by me are in reasonable agreement.

The one major difference between the SW calculations and mine is that SW predict the existence of a forbidden component of the λ4471 transition at 4517 Å. This prediction arises from the broadening theory of Griem (1968) which they use. The Barnard *et al.* (1969) theory, used here, does not predict the existence of this forbidden component, and consequently the line does not appear in my models. Until a line at 4517 Å is actually observed, it would seem best to ignore it in theoretical calculations as I have done.

The main difference between the metal-rich and the zero-metal models (see above) is that the metal-rich models look hotter than the zero-metal models of the same effective temperature. Thus $W(4471)$ is higher in the metal-rich models than in the corresponding zero-metal models. This effect is a result of the increase in opacity of the metal-rich models brought about by the increased electron density, as the absorption is almost all free-free absorption from He^-. The unusually low value of $W(4471)$ in the [22, 8; 1, 1] model is a result of the cutoff of the line at $\lambda = 150$ Å, which imposes artificial limitations on the equivalent width.

III. OBSERVATIONAL DATA

The observational foundation for this paper is an extensive set of observations of white dwarfs by Oke (1972). These observations were made with the multichannel spectrometer of the 200-inch (508-cm) Hale telescope (Oke 1969). For most of the DA stars, observations were obtained with a resolution of 20 Å; such a resolution is adequate to measure hydrogen line profiles. For a few DA stars, and for stars of other spectral types, the resolution was 80 Å—sufficient to measure equivalent widths. I obtained Hγ profiles of two stars (W485 A and He [=Hertzsprung] 3) at the Cassegrain scanner of the Mount Wilson 60-inch (152-cm) telescope.

The parallaxes used in this paper are listed in table 4, along with references. The stars are listed in order of spectral class (DA, DB, DO, cool DA, and peculiar types), and in order of right ascension within a spectral class. The order of spectral classes proceeds in order of increasing uncertainty in the deduced masses and radii. A full discussion of the parallaxes of white dwarfs was given 2 years ago by Eggen (1969).

In using the parallaxes in the literature, I have given each parallax a highly subjective rating based on the quoted probable error and the number and accordance of different determinations of an individual parallax. Crudely, parallaxes rated A have an estimated uncertainty of 10 percent or less; those rated B, 10–25 percent; C, 25–50 percent; while the D-rated parallaxes are of academic interest only. The total weight is the weight of all of the plates used in determinations from different observatories. I have used the classical value of the Hyades distance modulus, $m - M = +3.03$ (Wayman, Symms, and Blackwell 1965). The distance modulus of any individual Hyad is uncertain by about 0.3 mag owing to the depth of the cluster; this uncertainty is about the same order of magnitude as the change in the distance modulus proposed recently (e.g., van Altena 1969). Even with these uncertainties, the distances to white dwarfs in the Hyades are considerably better determined than the distance to most white dwarfs. I have assumed that HZ 2 is a Hyades member, following the arguments of Eggen (1969).

IV. PROCEDURES

Effective temperature, surface gravity, and abundance are the only parameters which are directly measurable from an analysis of the stellar spectrum. If the distance to the star is known, the mass and radius can be determined. In order to avoid the uncertainties inherent in the use of the bolometric correction, I calculated the radii of stars from the observed visual magnitudes and the monochromatic fluxes from the models. With an effective wavelength of 5480 Å for the V-filter (Allen 1963) and the usual definition of magnitudes, I find

$$2 \log (R/R_\odot) = -\log H_{5480} - 2 \log \pi - 1.221 - m_V/2.5 \quad (1)$$

where the logarithms are to base 10, H_{5480} is the flux at $\lambda = 5480$ Å from tables 1–3 (or tables 1A and 1B of Shipman 1971*b*) and is a number of order unity, π is the parallax, and m_V is the observed visual magnitude. The absolute flux calibration was that of Oke and Schild (1970). In practice, the dominant uncertainty in applying equation (1) is the uncertainty in the parallax; such errors as the error in the visual magnitude or the error in H_{5480} arising from the uncertainty in fitting the model to the real star are, in general, unimportant. Only when there is a major uncertainty as to choice of model does the uncertainty in H_{5480} become significant.

Once the radius is determined, the luminosity and mass can be found from two familiar equations:

$$\log (L/L_\odot) = 2 \log (R/R_\odot) + 4 \log (T_{\rm eff}/10^4) + 0.944\,, \quad (2)$$

$$\log (M/M_\odot) = \log g - 2 \log (R/R_\odot) - 4.44\,. \quad (3)$$

The values of these parameters are tabulated in table 4 for all of the stars in the observing program.

V. DA STARS WITH $T_{\rm eff} \geq 12{,}000°$ K

The DA stars are the simplest to analyze of all the white-dwarf types, in that it is possible to obtain a great deal of information from their spectra, and the basic physics used in the model-atmosphere calculations is well known. Effective temperatures can be obtained by comparing the energy distributions from the model and the star. The main determinant of effective temperature is the Balmer discontinuity, which for $T_{\rm eff} \geq 14{,}000°$ is almost completely independent of surface gravity. The fits were made mainly by eye, while the interpolation was facilitated by using a monochromatic color index $\Delta m = \mathrm{AB}(\lambda = 5560) - \mathrm{AB}(\lambda = 3600)$. Here $\mathrm{AB} = -2.5 \log F_\nu + \text{const.}$ This index is analogous to $-(U - V)$ in the UBV system.

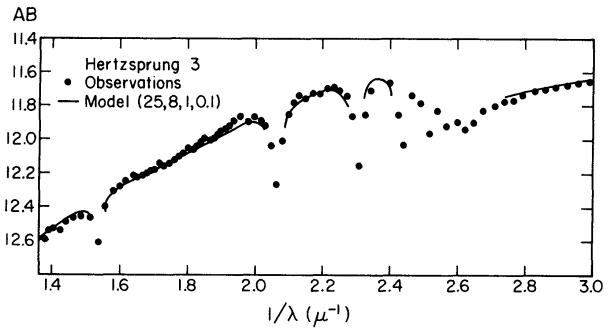

FIG. 1.—Observed and theoretical energy distributions for Hertzsprung 3, a DA star

In this way, effective temperatures can be determined with an uncertainty of about 5 percent. A typical comparison of model and observations is given in figure 1 for Hertzsprung 3. In each individual case, the errors quoted in table 4 were estimated from the goodness of fit, and are intended to be generous estimates of the probable error.

Once the effective temperature is known, the surface gravity is found by fitting hydrogen line profiles to the observations. Hβ and Hγ were used in the present case, since they were the easiest to observe and were not too badly confused by overlapping lines. One major problem in analyses of this sort is the matter of definition of the continuum. In order to eliminate, as much as possible, the systematic error inherent in the uncertainty of continuum placement, a self-consistent treatment of models and observations is needed. What the scanner does in looking at a star is to count all photons with

$$\lambda_c - \tfrac{1}{2}B < \lambda < \lambda_c + \tfrac{1}{2}B\,, \tag{4}$$

where λ_c is the central wavelength of the scanner observation, B the bandpass, and λ the wavelength of the photon. I therefore synthesized a set of theoretical scanner observations for each model by folding the theoretical profile with a rectangular instrumental profile of the appropriate width. The continuum was then found by drawing a straight line on a magnitude scale through the observed points at specified wavelengths for both the observations and the theoretical profile. The continuum wavelengths were $\lambda\lambda$4190, 4210, 4230, 4250, 4510, 4530, and 4550 for Hγ and $\lambda\lambda$4690, 4710, 4730, 4750, 5110, 5130, 5150 for Hβ. These wavelengths were chosen so that any possible influence on the continuum placement from He I $\lambda\lambda$4471 and 5015 would be eliminated, even though these lines were not seen.

The surface gravity can now be found by fitting theory to observation. Highest weight was given to the points at 30 and 50 Å from line center. In general, the uncertainty in the surface gravity was about 0.2 in the logarithm; error estimates in individual cases were made on the basis of goodness of fit. A sample profile is plotted in figure 2. The asymmetry in the observations is due to velocity shifts and guiding errors (1–2 Å) and should not be regarded as real. For stars with lower resolution scans, equivalent widths were measured from the scans and used to determine surface gravities, although with 40 Å resolution some comparison of profiles was possible. In all cases the self-consistent treatment of scan and model as described above was used.

Since hydrogen lines are the only lines visible in the spectra of DA stars, one can only assign upper limits to the abundance of other elements. In the case of helium, these upper limits can be quite stringent. He I λ4471 was not observed in any of the stars in table 4, and thus $W(4471) \lesssim 1$ Å on the basis of counting statistics. This

TABLE 4 - MASSES, RADII, AND ATMOSPHERIC PARAMETERS

Star	EG	Sp. Type	T_{eff}	log g	Parallax (0".001)	Quality (Total Wt.)	Source	log $M/M_\odot$	log $R/R_\odot$	log $L/L_\odot$
HZ 4	26	DA	15,300± 400	8.1 ±0.30	025±003	B	Hyad	-.09±.30	-1.92±.06	-2.16±.12
LB 1240	28	DA	13,800 500	7.5 0.30	036 003	C(20)	USNO	-.70 .30	-1.92 .05	-2.36 .10
LB 227	29	DA	16,500 500	8.3 0.30	025 003	B	Hyad	-.28 .30	-2.12 .06	-2.43 .12
HZ 2	31	DA	22,500 500	8.0 0.20	025 003	B	Hyad	-.20 .15	-1.92 .06	-1.48 .12
40 Eri B	33	DA	17,000 500	7.75 0.15	202 004	A(67)	J	-.35 .15	-1.88 .02	-1.90 .10
HZ 7	39	DA	23,000 500	7.9 0.20	025 003	B	Hyad	-.42 .20	-2.00 .06	-1.61 .12
HZ 14	42	DA	34,000 1000	8.5* 0.40	025 003	B	Hyad	-.02*.40	-2.04 .06	-1.01 .12
He 3	50	DA	25,000 700	8.1 0.15	060 010	B(35)	J	-.24 .22	-2.00 .07	-1.46 .14
SA 29-130	67	DA	14,500 500	8.0 0.30	032 003	C(28)	J,USNO	+.06 .40	-1.80 .10	-1.99 .30
L 970-30	76	DA	16,000 500	7.9 0.20	046	C	EG I	-.27 .30	-1.91 .10	-2.05 .20
GD 140	184	DAn	23,000 800	8.2 0.50						
W 485 A	99	DA	15,500 500	8.5* 0.30	062 006	B(31)	J,USNO	+.37*.30	-1.90 .07	-2.09 .14
+70°5824	102	DA	21,000 1000	7.7 0.30	027 012	D(7)	J	-.11 .50	-1.74 .25	-1.23 .40
GD 185	192	DAn	19,000 500	9.1 0.50						
W 1346	139	DA	20,000 700	7.3 0.30	072 010	B(59)	J,A	-.83 .15	-1.89 .07	-1.64 .14
+73°8031	144	DA	16,000 500	7.7 0.30	045 010	D(9)	A	-.40 .35	-1.88 .08	-2.00 .16
L 1512-34B	162	DA	14,000 300	7.9 0.30	069 015	C	A*	-.49 .35	-2.03 .07	-2.52 .14
LDS 235B	63	DB	15,000 1000	8.0:	011	C	EG I	0.0:	-1.78 .05	-1.80 .20
Ton 573	77	DB	14,000 1000							
GD 190	193	DB	18,000 2000	8.5 ±1.0						
L 1573-31	133	DB	15,000 1000							
LDS 749 B	145	DB	14,000 1000	7.5 0.6	021 003	C(16)	USNO	-.60±.60	-1.83 .10	-2.12 .20
L 930-80	149	DB	16,500 1000	8.0 0.5	052 015	D-	G*	-1.12:	-2.34:	-2.80:
F 24	20	DAwk	50,000+	6.6+						
G 191		sdO	50,000+	6.0+						
HZ 21	86	DO	70,000+	8						
HZ 43	98	DAwk	50,000±5000	8.8±1.0	021 011	D(10)	A	+.60±1.0	-1.83±.25	-0.02±.50
HZ 44*		sdO	50,000 5000	6.5 1.0						
L 870-2	11	DA	6,500 500		061 013	C(6)	J		-1.41 .15	-2.63 .40
L 745-46A	54	DF	5,000(1)		146 007	B(15)	J		-1.56(1)	-3.39(1)
			7,000(2)						-2.01(2)	-3.68(2)
R 627	79	DA,F	7,000± 500		074 010	C(23)	J,USNO		-1.86±.07	-3.38±.40
R 640	119	DF	6,000(1)		056 007	C(15)	A		-1.53(1)	-3.00(1)
			8,000(2)						-1.80(2)	-3.06(2)
G 99-37	248	DGp	5,000(1)							
			7,000(2)							
G 47-18	182	λ4670	10,000(1)		032	C	E		-1.94(1)	-2.94(1)
			12,000(2)						-2.07(2)	-2.90(2)
+70°8247	129	λ4135	12,000:		081 010	B(24)	Yk		-2.08:	-2.90
L 1363-3	148	DC	6,000(1)		074 004	C(17)	USNO		-1.50(1)	-2.94(1)
			8,000(2)						-1.67(2)	-2.81(2)

NOTES TO TABLE 4

REFERENCES. A, Wagman (1967); E, Eggen (1969); EG I, Eggen and Greenstein (1965*a*); G, Gliese (1969, his source is Wagman 1965); J, Jenkins (1963); USNO, Riddle (1970); Yk, van Altena (1971). E and EG I obtain distances from proper-motion companions.

For L745–46 A, R640, G99-37, G47-18, and L1363-3, parameters denoted by (1) are derived under the helium-rich assumption, and those denoted by (2) are based on the blackbody assumption.

NOTES ON SPECIFIC STARS.

HZ 14.—The surface gravity is an average of determinations from the scan and Graham's (1969) m_1-index.

W485 A.—The m_1-index is consistent with $\log g = 8.5$.

L1512-34 B.—Wagman gives $\pi = 0''.057$, while EG I give $\pi = 0''.080$ from the brightness of L1512-34 A. I have used the mean.

L930-80.—This parallax, based on only nine plates, is extremely uncertain.

HZ 44.—Peterson (1969) finds $T_{\rm eff} = 40{,}000°$, $\log g = 5.7$ with $N(\rm He) = 0.40$ by number.

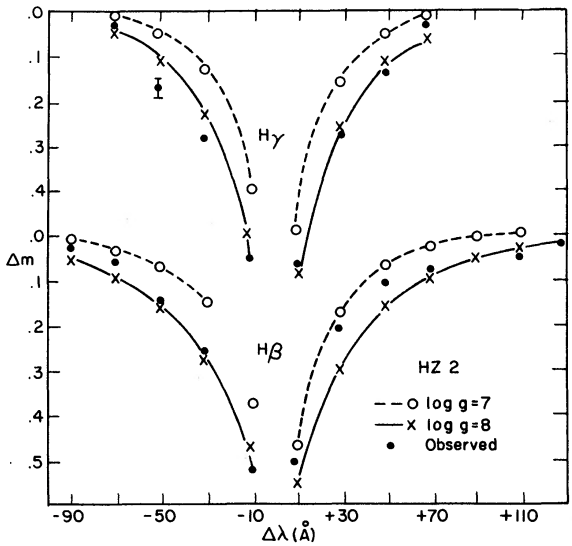

FIG. 2.—Hydrogen line profiles for HZ 2. The ordinate is in magnitudes.

limit corresponds to three times the standard deviation. At $T_{\rm eff} = 25{,}000°$, $W(4471) = 1$ Å corresponds to a helium abundance of 0.2 percent if λ4471 is on the square-root part of the curve of growth, and 0.75 percent if the linear part of the curve of growth is applicable. For other temperatures, these limits are less stringent. At any rate, one can definitely say that for He 3 ($T_{\rm eff} = 25{,}000°$) the helium abundance is certainly less than 1 percent by number. Since the surface gravities given in table 4 correspond to the assumed helium abundance of the models, 10 percent by number, these gravities were increased by 0.1 in the log before the mass was calculated to account for the difference in helium abundance between the model and the real star (Matsushima and Terashita 1969*a*). Because of the weakness of metal lines in white dwarf spectra (see SW), it is only possible to say that the DA stars have at most twice the solar abundance of metals.

Two of the DA stars listed in table 4 are good candidates for future parallax programs—GD 140 and GD 185. If they are assumed to lie on the mass-radius relation for helium, GD 185 has a mass barely under the Chandrasekhar limit, a radius of $0.004R_\odot$, and a parallax of $0''.03$, while GD 140 has $R = 0.013R_\odot$, $M = 1.2M_\odot$, and a parallax of $0''.04$. For both of these stars, the surface gravity is uncertain because the resolution of the scans was 80 Å. These two stars are worthy of more investigation.

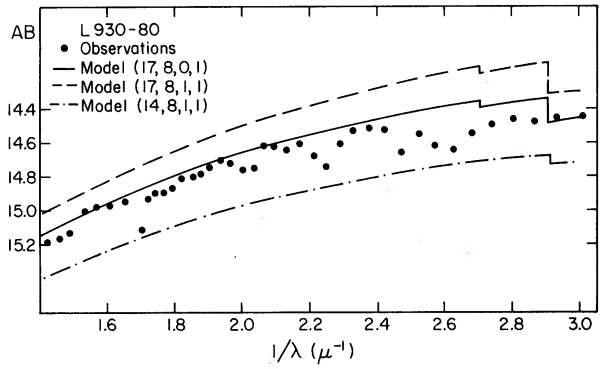

FIG. 3.—Observed and theoretical energy distributions for L930-80, a DB star

VI. DB STARS

The DB stars are considerably more difficult to analyze than the DA stars, primarily because the spectra give more sketchy information about the effective temperature and no reliable information about the surface gravity. The effective temperatures of DB stars were determined by fitting energy distributions to models. The main temperature-dependent features were the slope of the visual continuum and the size of the discontinuity around 3600 Å, which is caused by the discontinuities at 3422 and 3680 Å arising from the $n = 2$ levels of helium. A comparison between the observations and various theoretical models for L 930-80 is shown in figure 3.

It is apparent from figure 3 that the assumed value of the metal abundance affects the deduced temperature of the star. Changing the metal abundance affects the electron density, which affects the absorption coefficient and thus the temperature gradient as discussed earlier (§ II). The difference in the effective temperatures deduced from the solar-metal and zero-metal models is about 1000°, which is comparable to the uncertainty arising from the fitting procedure. The temperatures given in table 4 are averages of the determinations from the solar-metal and zero-metal models.

Unfortunately, the helium line strengths are almost independent of surface gravity, because the line and continuum absorption coefficients are both linearly dependent on the electron density. In a few cases I estimated the surface gravity by the shape of the helium line, because the lines become broader (but not stronger) as the gravity increases. These determinations of surface gravity should be given very low weight. However, it was possible to use the helium line strengths as a check on the temperature determinations; in all cases the agreement of the line-determined temperature with the

TABLE 5

HELIUM LINE STRENGTHS

	STAR					
He I λ(Å)	+70°8247	LDS 235 B	GD 190	L1573-31	LDS 749 B	L930-80
4026.....	3	blend	blend	14.2	4.7	9.6
4471.....	6.5	22.7	32.6	16.2:	6.0	22.0
4922.....	2	...	...	...	5.1	...
5015.....	6.3	14.2*	24.3*	14.2*	4.8	17.6*
5876.....	11.7	39	22.8	12.4	6.2	13.6

NOTE.—The resolution of the scans used in these measurements was 20 Å for LDS 749 B, 40 Å for +70°8247, and 80 Å for the others.

* Blend of λλ4922 and 5015.

continuum-determined temperature was consistent with the large errors involved. The helium line strengths measured from the scans are listed in table 5.

Because the continuum absorption in DB stars is much less than that of DA stars, it is possible to set more stringent limits on the abundance of metals and hydrogen. Bues (1970) has estimated that $N(\mathrm{H}) \lesssim 10^{-5}$. If we apply a generous upper limit of 2 Å for the width of Ca II H and K from the observations, the calculations of SW indicate that in LDS 749 B with $T_{\mathrm{eff}} \approx 14{,}000°$ calcium is underabundant (with respect to the total number of atoms) by at least a factor of 25, if the linear part of the curve of growth is applicable. If, as is more likely, the square-root part is applicable, this factor becomes 10^3; 10^2 is a reasonably safe average.

The masses given in table 4 for DB stars are very approximate, but the radii are somewhat better determined as they are less sensitive to model details. More astrometric data are needed for these stars; in particular, another measurement of the apparently large parallax of L930-80 would be most useful. The analysis of the DB stars is only beginning.

VII. HOT WHITE DWARFS

Determination of effective temperatures for hot ($T_{\mathrm{eff}} \lesssim 35{,}000°$) white dwarfs is quite difficult. The main indicator of temperature is still the Balmer discontinuity, although the slope of the Paschen continuum provides a secondary temperature-dependent feature. The error in $\theta_{\mathrm{eff}}(=5040/T_{\mathrm{eff}})$ is only 0.02, twice that for cooler stars; but this error corresponds to a much greater error in T_{eff} at high temperatures (small θ). All the hot stars in table 4 have been analyzed with the assumption that helium is a negligible constituent of their atmospheres; serious errors will arise only if $N(\mathrm{He})$ is substantially greater than about 20 percent, as is the case for HZ 44. The surface gravities are determined in the same way as for the DA stars, but the uncertainties are very large. The five hot stars listed in table 4 are quite heterogeneous; not all of them are genuine white dwarfs.

VIII. COOL WHITE DWARFS

It is possible to determine the temperatures of the cool, hydrogen-rich stars (L870-2 and Ross 627) fairly accurately since the absorption coefficient in their atmospheres, that of hydrogen, is accurately known. Unfortunately the hydrogen line strengths are almost completely independent of surface gravity (see § II above), so that there is no way to determine the mass of these objects. It is possible to estimate crudely the metal abundance of these stars from the Ca II K-line width. The line and continuum absorption coefficients are both linearly dependent on the electron density. Since the equivalent width of the line is a function of the ratio of these two absorption coefficients, the calcium line strengths are independent of surface gravity in the same way as the hydrogen line strengths. Thus the K-line strength in white dwarfs should be approximately the same as in main-sequence stars of the same effective temperature: 10 Å at $T_{\mathrm{eff}} = 6000°$ (Wright *et al.* 1964). The K-line strength is 1 Å in Ross 627 and is not observed (< 1 Å) in L870-2. Thus Ca is underabundant by a factor of 100 in Ross 627, and by at least this factor in L870-2, if the square-root part of the curve of growth is applicable in this equivalent width range. If the linear part of the curve of growth is applicable, the upper limit is 0.1 of the solar abundance.

The radius of Ross 627 is approximately the same as the radii of the DA white dwarfs discussed in § V, but the radius of L870-2 is greater by a factor of 3. I do not believe that this difference can be ascribed to errors, as either the temperature would have to be increased from 6500° to 14,000° or the parallax would have to be increased from 0″.061 to 0″.18. These changes are beyond the bounds of possible error.

There are a variety of hydrogen-poor, cool white dwarfs at the end of table 4. One determines effective temperatures for these stars by comparing observed and model energy distributions, but an ambiguity arises because one does not know the major constituent of their atmospheres. Most plausible constituents like H, C, N, or O can be ruled out, since their presence would be revealed by lines. The most reasonable assumption is that these stars are mostly helium, since helium lines are invisible at these low temperatures. I have listed two effective temperatures in table 4 for each star: one based on the helium-rich atmospheres of § II and a blackbody temperature. The true value should probably lie in the range of these two temperatures.

The metal abundances of these stars are quite peculiar. A simple-minded square-root-part-of-the-curve-of-growth approach leads to an upper limit of $\frac{1}{400}$ times the solar value for the Ca abundance of the DC star L1363-3. The DF stars have Ca abundances of $\frac{1}{25}$ and $\frac{1}{900}$ the solar value, respectively. These numbers are only order-of-magnitude estimates as the models are quite inadequate. The analysis of the magnetic white dwarf Grw+70°8247 is based on a presumed identification of most of the spectrum lines as helium; although most of the helium spectrum is present in this star, the relative strengths of the lines are quite different from those of other DB stars. While Angel's (1972) proposed identification of the λ4135 feature in this star's spectrum as He_2 supports the hypothesis that +70°8247 is composed of helium, the data listed in table 4 for this star should be regarded as tentative.

While the results for the hydrogen-rich stars Ross 627 and L870-2 are fairly reliable, the present analysis of hydrogen-poor white dwarfs is quite primitive. Wegner (1971) has found effective temperatures of 7800° K for L745-46 A and 7130° K for Ross 640 by matching broad-band colors and line profiles to a more detailed grid of model atmospheres than the ones presented here. It is encouraging that his more detailed analysis leads to temperatures in general agreement with the present values. More work, both observational and theoretical, is needed on the hydrogen-poor white dwarfs.

IX. BOOTSTRAPPING: TEMPERATURE SCALES AND RADII

Now that the reliable effective temperatures have been obtained for a considerable number of white dwarfs, it is possible to calibrate the broad-band *UBV* observations and establish a reliable temperature scale. In this way one can obtain information about stars which have not been observed by the multichannel, and conclusions about the statistical makeup of white dwarfs can rest on a larger sample. The problem of defining an adequate temperature scale has been called "an astrophysical puzzle" by Greenstein and Trimble (1967; hereafter referred as GT) in view of the large discrepancies between the then-existing temperature scales.

The relation between the effective temperature and $U - V$ color of the DA and DA,F stars listed in table 4 is plotted in figure 4. The smooth solid curve denotes the temperature scale proposed here for the hydrogen-rich white dwarfs. The other curves represent other temperature scales discussed by GT. "TM" refers to the temperature scale of Terashita and Matsushima, which was based on computation of *UBV* colors directly from models. "W" refers to the temperature scale of Weidemann (1963), who determined effective temperatures from the central depths of hydrogen lines and approximate model atmospheres. "GT" refers to the scale originally proposed by Eggen and Greenstein (1965; hereafter EG I) which was established by interpolating between the main sequence and the blackbody line in the two-color diagram. The present temperature scale has a firmer basis than any of the previous ones.

One consequence of the nonlinear temperature scale of figure 5 is that the upper sequence of Eggen (1969), which is a straight line on an (M_V, $U - V$)-diagram, is no longer a straight line on a ($\log L$, $\log T_{\rm eff}$)-diagram. The cool ($T_{\rm eff} \lesssim 8000°$) white dwarfs of Eggen's upper sequence will have $R \gtrsim 0.04 R_\odot$, while the hotter members

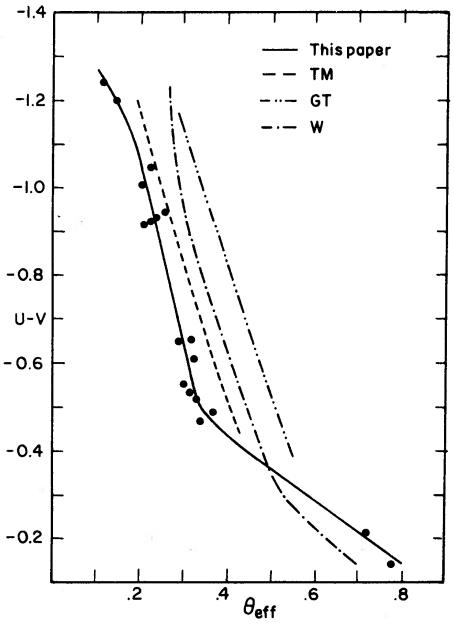

FIG. 4.—Temperature scales for DA stars. The dots are from table 4. The other temperature scales shown here are described in the text.

have $R \sim 0.01 R_\odot$. While the observational evidence pertaining to the two-sequence hypothesis is unclear (cf. Weidemann 1968), the great disparity in radii between hot and cool upper-sequence white dwarfs renders the idea of a physical connection between the two somewhat less attractive. Furthermore, the agreement between Eggen's sequences and the crystallization sequences of Van Horn (1968) is jeopardized by the new temperature scale, as the Van Horn sequences are straight lines in the ($\log L$, $\log T_{\rm eff}$)-diagram.

I have also attempted to define a ($U - V$, $T_{\rm eff}$)-relation for the DB and DC stars in the same way as for the DA stars (fig. 5). This temperature scale is quite crude because of the shortage of observed points, and it can be regarded as reliable only for $T_{\rm eff} \gtrsim 11{,}000°$ (the solid part of the curve). The dotted part of the curve uses the helium-rich, rather than the blackbody, temperatures of § VIII.

Using the temperature scales of figures 4 and 5, I have calculated temperatures, radii, and luminosities for all stars in the Eggen-Greenstein lists (Eggen and Greenstein 1965*a*, *b*, 1967; Greenstein 1969*a*, *b*, 1970) with known distances. These data are listed in table 6. The parallaxes are taken from the compilation of Eggen (1969), except for the Praesepe stars LB 390, LB 1847, and LB 393, which are from EG I. Riddle's (1970) parallaxes were also used where noted.

The stars in table 6 are put into error classes based on the quality of the parallaxes. The first-class determinations are those which have uncertainties in the radii of less than 0.08 dex (about 25 percent) and are analogous to classes A and B of table 4. These distances are derived from (i) large parallaxes measured at more than one observatory (table 1 of Eggen 1969), (ii) common-proper-motion (cpm) pairs with the non–white dwarf a main-sequence star bluer than $B - V = +1.2$ (Eggen's table 2), and (iii) Hyades and Praesepe stars. The second-class determinations have radii accurate to better than 0.15 dex (41 percent), which corresponds to an error of 0.75 in M_V, and they are analogous to the C class of table 4. They are bases on trigonometric parallaxes greater than 0".03 and cpm pairs containing a very red dwarf (Eggen's tables 4 and 6 and some stars from Riddle 1970). The third-class determinations corre-

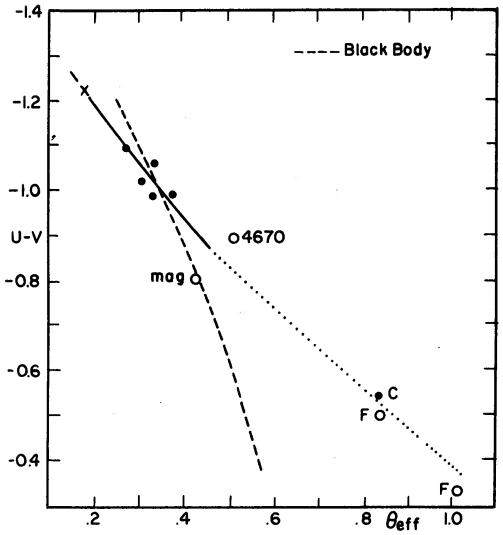

FIG. 5.—Temperature scales for DB and DC stars. *Dots*, DB stars; *cross*, HZ 29, which may not be a white dwarf. *Open circles*, other spectral types: "F" are DF stars, "mag" is Grw+70°8247, and "4670" is G47-18. Only the dots were used to determine the temperature scale (*solid line*), the dotted portion of which is very uncertain. The blackbody line is from Mathews and Sandage (1963).

spond to the D class of table 4, and include trigonometric parallaxes from Eggen's table 7 which are larger than 0".01.

Radii were computed with the procedures of § IV. Photometry was from the Eggen-Greenstein lists or, in a few cases, from Eggen (1969). If the spectrum of the star was unclassified, it was assumed to be a DA. The median radius of the stars in table 6 is $0.0095R_\odot$, somewhat less than the mean radius of $0.013R_\odot$ for the stars in table 4. The stars in table 4, from Oke's observing program, were in general selected from the brightest white dwarfs, so that table 6 is probably a more representative sample.

X. BOOTSTRAPPING: MASSES

One can also compute masses for a few more DA stars than those listed in table 4. Graham (1969, 1972) has done *ubvy* photometry for a large number of white dwarfs. The m_1-index, defined by

$$m_1 = (v_{4100} - b_{4670}) - (b_{4670} - y_{5500}), \tag{5}$$

where the subscripts indicate the central wavelength of the relevant filter, is a useful indicator of Hδ strength in white dwarfs. Since most of the stars listed in table 4 were also observed by Graham, it is possible to calibrate his m_1-indices in terms of a hydrogen-line equivalent width. I used theoretical equivalent widths, calculated from the values of $T_{\rm eff}$ and $\log g$ in table 4, as the basis for the calibration. Observational equivalent widths from the scans are inaccurate because of the high weight given to points near line center, which are affected by guiding errors. In this way, surface gravities and masses were computed for the stars in table 7.

The uncertainties listed in the table are largely due to observational errors, and were estimated from the scatter in the calibration curve. One noteworthy star in table 6 is LDS 678 B, which has hydrogen lines that are too weak for its color by a factor of 6 as determined by the m_1-index. The photographic hydrogen line strengths are also unusually small. This star is probably underabundant in hydrogen, as its radius is

Table 6

Luminosities and Radii

Star	Spec.	EG	M_V	θ_{eff}	log $R/R_\odot$	log $L/L_\odot$
First-Class Determinations						
LDS 678B#	DAwk	131	+12.2	.267	-2.14	-2.26
L 997-21	DAs	135	+13.5	.500	-2.20	-3.22
L 326-81	DAs	165	+13.4	.262	-2.38	-2.69
G 94-B5B	DAn	18	+12.5	.295	-2.17	-2.48
G 102-39	DC	44	+12.9	.63	-1.83	-3.10
G 116-16	DAs	64	+11.7	.57	-1.64	-2.56
-37°6571	DAs	114	+12.2	.90	-1.85	-2.76
G 140-B1B	DC	124	+12.9	.66	-1.77	-3.08
G 165-B5B	DA	173	+12.0	.305	-2.06	-2.30
G 156-64	DA,F	178	+14.2	.93	-1.70	-3.54
LDS 157C	--	--	+12.2	.200	-2.23	-1.97
HZ 10	DA	30	+11.1	.440	-1.71	-2.21
VR 7	DA	36	+11.6	.250	-2.04	-1.92
VR 16	DA	37	+11.0	.200	-1.98	-1.45
LP 475-242	--	--	+11.9	.205	-2.16	-1.82
LB 390	--	59	+12.2	.300	-2.11	-2.36
LB 1847	--	60	+12.6	.375	-2.11	-2.76
LB 393	--	61	+12.1	.320	-2.07	-2.39
Second-Class Determinations						
LP 9-231*#	DAss	199	+12.9	.72	-1.70	-3.06
R 198	DA	143	+13.4	.335	-2.32	-2.97
+82°3818	DA	147	+11.6	.275	-2.01	-2.02
-51°13128B	--	--	+13.7	.290	-2.42	-2.94
G 130-49	--	1	+13.4	.375	-2.27	-3.08
G 71-B5B	--	14	+13.0	.308	-2.25	-2.70
G 86-B1B	DA	43	+12.8	.525	-1.94	-3.01
G 105-B2B	--	47	+13.3	.345	-2.28	-2.96
G 148-7	DAn	83	+11.1	.295	-1.89	-1.92
LDS 455B	DA	101	+12.0	.242	-2.13	-2.04
G 152-B4B	DAs	174	+11.2	.330	-1.88	-2.08
G 154-B5B	DA	175	+11.2	.82	-1.25	-2.39
G 148-7	DAs	185	+11.1	.305	-1.87	-1.97
W 1516@	DC	9	+12.7	.630	-1.80	-3.02
G 93-48@	DA	150	+10.7	.265	-1.84	-1.62
G 29-38@	DA	159	+12.4	.500	-1.88	-2.82
Third-Class Determinations						
+25°6725#	DA	15	+10.1	.240	-1.76	-1.30
h Per 1166	DA	17	+10.6	.205	-1.91	-1.32
R 808	DA	115	+11.1	.44	-1.72	-2.26
C 2	DA	116	+10.8	.355	-1.76	-1.99
R 137#	DA	125	+10.1	.245	-1.75	-1.31

Notes

*LP 9-231: The colors are from Eggen (1969). The colors in EG III lead to θ_{eff}=.90, log $R/R_\odot$=-1.42, and log $L/L_\odot$= -2.90, but the more recent colors of Eggen were used here.

#LDS 678B, LP 9-231, +25°6725, R 137: In addition to the parallaxes quoted by Eggen, the work of Riddle (1970) was also used in the determination of distances.

@W 1516,G 93-48, G 29-38: Parallaxes from Riddle (1970).

TABLE 7

MASSES FROM m_1-INDICES

Star	m_1	log g	log $M/M_\odot$
G165-B5 B.....	+0.317	7.9 ± 0.4	−0.56 ± 0.4
HZ 10.....	+0.358	8.0 ± 0.4	+0.01 ± 0.4
VR 7.....	+0.275	7.6 ± 0.4	−0.70 ± 0.4
VR 16.....	+0.245	7.7 ± 0.4	−0.52 ± 0.4
+82°3818.....	+0.290	7.6 ± 0.4	−0.76 ± 0.4
G148-7.....	+0.347	7.9 ± 0.4	−0.22 ± 0.4
G152-B4 B.....	+0.312	7.7 ± 0.4	−0.46 ± 0.4
R808.....	+0.312	7.7 ± 0.4	−0.13 ± 0.5
C2.....	+0.344	7.8 ± 0.4	−0.02 ± 0.5

well determined, and deserves detailed study. The median mass of all the stars in tables 4 and 7 is $0.52M_\odot$, which is quite close to the estimated mass of 0.5–$0.6M_\odot$ for the horizontal-branch stars (Demarque and Mengel 1971 and references therein). Trimble and Greenstein (1972) have estimated $M \sim 0.79M_\odot$ for a somewhat different sample of white dwarfs using the temperature scale of figure 4 and gravitational-redshift results. In view of the difference in samples and the systematic errors which may be present in both procedures, this discrepancy is not serious.

XI. COMPARISON WITH GRAVITATIONAL-REDSHIFT RESULTS

It is possible, in a few cases, to compare the masses and radii derived by model-atmosphere methods with masses derived from binary-star orbits or from measurement of gravitational redshifts. Such a comparison provides an important check on the possibility of systematic errors in the model-atmosphere method.

The classic comparison case is the white dwarf 40 Eri B. Of the three white dwarfs whose masses have been measured by the analysis of binary-star orbits, it is the only one which is fully accessible to spectroscopic observation. The dynamical mass is $0.43 \pm 0.10M_\odot$ (van den Bos 1960),[1] while the model-atmosphere mass is $0.45 \pm 0.13M_\odot$. Furthermore, Popper (1954) has made a highly accurate measurement of the gravitational redshift of 40 Eri B, finding $k = +21 \pm 4$ km s^{-1}, while the mass and radius listed in table 4 yield $k = +22$ km s^{-1}. In both cases the agreement is excellent. 40 Eridani B is not typical of the stars in table 4, since the observations of this star are of much higher quality than the observations of any other star listed in this paper. However, the excellent agreement of the model-atmosphere results with the work of van den Bos and Popper does indicate that the systematic errors are not large.

Extensive measurements of gravitational redshifts have been made by Greenstein and Trimble (GT; Trimble and Greenstein 1972). When a star's radial velocity is known because of its membership in a stellar system, a direct comparison of gravitational-redshift and model-atmosphere results is possible. Such a comparison of the redshifts measured and the redshifts predicted from the masses of tables 4 and 7 is made in table 8. The mean value of $k_{\text{atmospheric}} - k_{\text{GT}}$ of -19 km s^{-1} does not represent a serious discrepancy, as the discussion in GT indicates that such a systematic error would be entirely possible. It is also possible that the gravities in tables 4 and 7 are too low by 0.12 in the log, which would explain the discrepancy.

Another possible source of the difficulty is the existence of Stark shifts, mentioned by Wiese and Kelleher (1971). They contend that about 10 km s^{-1} of the redshift in a

[1] Dr. K. Kamper of the Van Vleck Observatory has kindly supplied me with this error estimate, which is somewhat greater than is commonly supposed.

TABLE 8

REDSHIFTS

Star	$k_{\text{atmosphere}}$	k_{GT}	$k_{\text{atm}} - k_{\text{GT}}$
HZ 4.....	+48(+40, −20)	+69 ± 20	−21
LB 1240.....	+20(+20, −10)	+52	−32
HZ 10.....	+48(+50, −25)	+43	+ 5
HZ 2.....	+36(+12, −9)	+27	+ 9
HZ 7.....	+25(+12, −9)	+79	−54
HZ 14.....	+55(+90, −32)	+65	−10
W1346.....	+ 7(+3, −2)	+38	−31
Mean.....			−19

white-dwarf spectrum is a pressure shift. If true, the discrepancies of table 8 would be reduced to 10 km s^{-1}. More work is needed on the problem of pressure shifts, since the data of Wiese and Kelleher are somewhat noisy for such small shifts. Furthermore, their estimate of the electron density in the stellar atmosphere at the point where Hγ is formed may be a little high. In any event, considering all the uncertainties, there seems to be no serious conflict between the gravitational-redshift data and the model-atmosphere results.

XII. MASS-RADIUS RELATIONS

One can also compare the masses and radii of tables 4–6 with the mass-radius relation for degenerate configurations. The mass-radius relation is not uniquely defined owing to possible thermal effects, uncertainty of composition, and effects of rotation. A comparison of the model-atmosphere results and various mass-radius relations is shown in figure 6. The Sirius B point is from Greenstein, Oke, and Shipman (1971). The points from GT are based on their mean redshifts for a large sample of stars.

The only highly accurate points in figure 6 are those for 40 Eri B and Sirius B. For the other stars, it is encouraging that, with the exception of HZ 43 and W485 A, the two points on the extreme right-hand edge of the diagram, all stars fall within a distance of one probable error from the Hamada-Salpeter (1961) mass-radius relation. It would clearly be premature to say that HZ 43 and W485 A are examples of rapidly rotating white dwarfs with masses above the Chandrasekhar limit, for the uncertainties in the masses of these stars are considerable.

XIII. EVOLUTION OF WHITE DWARFS

The first conclusion about white-dwarf evolution is suggested by the existence of cool white dwarfs such as L870-2 which have fairly large radii. The existence of extremely red ($U - V > +1$) subluminous stars with radii greater than typical white-dwarf radii was noted earlier by Eggen and Greenstein (1967). Since it is unlikely that a cooling white dwarf will expand, it is difficult to imagine that stars such as L870-2 and the large red subluminous stars are the evolutes of typical DA stars. Hence the present results would support the suggestion of Chin and Stothers (1971) that these cool white dwarfs have evolved directly from the giant stage along an almost vertical track in the H-R diagram, rather than following some track similar to the Harman-Seaton (1964) path for the nuclei of planetary nebulae.

The major problem in white-dwarf evolution, however, is explaining the existence of separate groups of white dwarfs with different atmospheric compositions. Strittmatter and Wickramasinghe (SW) have suggested two hypotheses to try to explain the

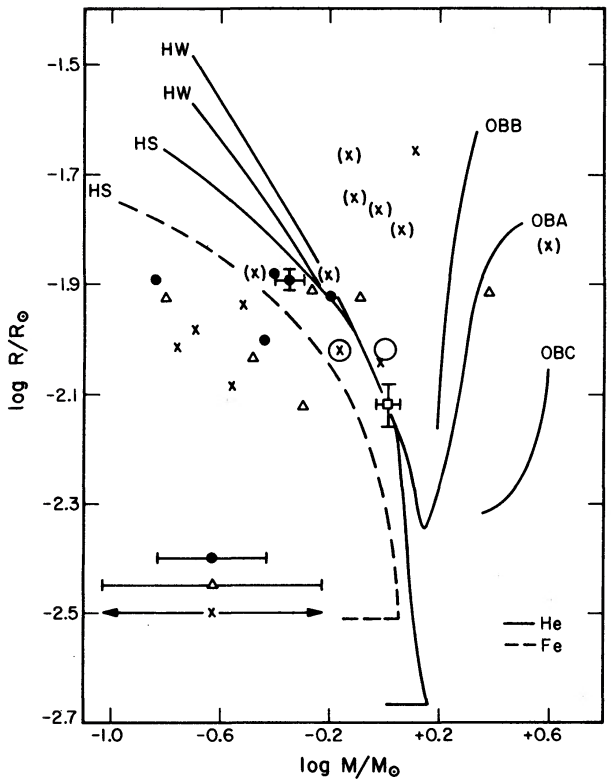

FIG. 6.—Mass-radius relations. The dots, triangles, and crosses represent three classes of uncertainties in the mass; the error bars indicate the maximum error within each group. Points in parentheses are those with less certain parallaxes (errors in log $R/R_\odot$ between 0.09 and 0.18). The dot with error bars is 40 Eri B, and the square with error bars is Sirius B. The large circle is the mean mass and radius from the mean gravitational redshift of GT; the crossed circle represents a reduction of their mean redshift by 19 km s^{-1}. The theoretical mass-radius relations referred to are: HS, the zero-temperature relations of Hamada and Salpeter (1961); HW, the finite-temperature relations of Hubbard and Wagner (1970); and OBA, OBB, and OBC refer to the rotating white-dwarf models of Ostriker and Bodenheimer (1968).

existence of the DB stars. As hypothesis A, which I discuss here, they propose that a white dwarf with a helium-rich interior cools as a DA because it accretes hydrogen from the interstellar medium. When it reaches the region of the H-R diagram in which the DB stars have convectively unstable atmospheres, SW assert that it will become a DB star, since the convection mixes the subsurface layers with the atmosphere. It continues to cool as a DB until convection ceases, when the star cools as a DA again.

SW predict as the principal observational consequence of their hypothesis A that there will be a deficiency of DA stars in the region $15{,}000° \leq T_{\rm eff} \leq 18{,}000°$ K, or $0.325 \geq \theta_{\rm eff} \geq 0.275$. This prediction is contradicted by the present results. Of the 18 DA stars listed in table 4, which have highly accurate temperatures, six have $15{,}000° \leq T_{\rm eff} \leq 18{,}000°$. I also calculated effective temperatures of all the stars in the Eggen-Greenstein lists using the temperature scales of figures 5 and 6. Of the 131 DA stars with $T_{\rm eff} \leq 50{,}000°$ K, 21 have values of $\theta_{\rm eff}$ in the "forbidden" range $0.325 \geq \theta_{\rm eff} \geq 0.275$, while 23 have $\theta_{\rm eff}$ values in the neighboring range $0.275 \geq \theta_{\rm eff} \geq 0.225$. Thus there is no evidence for a shortage of DA stars in the forbidden temperature range, as predicted by SW.

However, it is possible to modify the SW hypothesis A so that it is physically more plausible and so that it agrees with the observations. I propose here that a DA white

dwarf, which has accreted its surface hydrogen from the interstellar medium, will cool until $T_{\rm eff} \sim 13{,}000°$ K, when a hydrogen convection zone becomes established. SW's idea that a DA star will establish a helium convection zone at $T_{\rm eff} \sim 18{,}000°$ K is not self-consistent, as the atmospheres of DA stars contain little or no helium. If the surface hydrogen layer, accreted from the interstellar medium, is sufficiently thick, the bottom of the hydrogen convection zone will lie in a hydrogen-rich layer. Thus the surface composition of the star will be unaffected by convective mixing, and the star will continue to cool as a DA.

However, if the accreted surface layer is sufficiently thin, the hydrogen convection zone will extend downward to a layer which has not been accreted from the interstellar medium. If this layer is composed of helium, then helium will be mixed with the surface layers and the star will become a DB. The opacity of the surface layers is *decreased*, and the stellar surface becomes hotter. Hence the DB star will have a higher surface temperature than its DA ancestor.

It is possible to estimate the temperature increase which occurs when a DA white dwarf evolves into a DB. Starting with the stellar-interior equation

$$\frac{dT}{dr} = -\frac{3}{4ac}\frac{\kappa\rho}{T^3}L_r\,, \tag{6}$$

one can integrate this equation inwards from the surface of the star. Let the surface temperature be $T_{\rm eff}$, the interior be T_i, $L_r = 4\pi R^2\sigma T_{\rm eff}{}^4$, and

$$T_{\rm eff} - T_i = -\frac{3}{4ac}\left\langle\frac{\kappa}{T^3}\right\rangle\sigma T_{\rm eff}{}^4\int 4\pi R^2\rho dr\,. \tag{7}$$

With $T_i \gg T_{\rm eff}$, $\langle T^3\rangle = (T_i/2)^3$, $M_r = \int 4\pi R^2\rho dr$, and some algebra, one obtains

$$T_{\rm eff} = T_i\left[\frac{4ac}{3\langle\kappa\rangle M_r}\right]^{1/4}. \tag{8}$$

Hence, for a constant value of T_i, $T_{\rm eff} \propto \langle\kappa\rangle^{-1/4}$. From the appropriate models from § II, $\langle\kappa_{\rm Rosseland}\rangle(X = 1) \approx 5\langle\kappa_R\rangle(Y = 1)$, for $\tau = 1$. Thus a DA star with $T_{\rm eff} = 13{,}000°$ K will evolve into a DB star with $T_{\rm eff} = 19{,}000°$ K. Using the temperature scale of figure 5, I find that the hottest DB in the EG lists has $T_{\rm eff} = 20{,}000°$ K, with the exception of HZ 29 (which may not be a white dwarf). This agreement is excellent, considering the crudeness of the above calculation.

The lowest effective temperature of the DB stars in the EG lists is 11,000° K. From the models in § II, it is apparent that the existence of this low-temperature cutoff can be explained by the weakness or absence of helium lines at lower temperatures. Since, with the exception of EG 272, all DC stars are redder than $U - V = -0.71$, and hence cooler than $T_{\rm eff} \approx 8000°$ K (fig. 5), it seems attractive to suppose that DC stars are cooled-off DB stars.

If the atmospheres of the DB and DC stars are to remain hydrogen-poor, as is required by the present hypothesis, some way must be found to remove accreted hydrogen from the surface continuously. In the DB stars this removal can be accomplished by the surface convection layer, as the timescale for convective mixing is very short (see SW). In the DC stars, however, He is neutral at the surface, and the helium convection zone only exists below $\tau = 3$. Ordinary diffusion (not to be confused with differential gravitational settling) will suffice to mix accreted matter with the top of the convective layer, as the diffusion timescale is on the order of 10^4 seconds, and the time needed for a DC star to accrete a new atmosphere is 10^{10} seconds if Eddington's formula (cf. Danby and Camm 1957) is valid.

The objectives of the present modification of SW's hypothesis A are limited to

explaining (i) that the DB stars have $11{,}000° \leq T_{\rm eff} \leq 18{,}000°$ K and (ii) that the DC stars exist and are all cooler than the DB stars. These objectives are attained. The present hypothesis, and SW's hypothesis A, do not attempt to explain the low metal abundances of DB and DC stars. The solution to the metal-abundance problem may well lie in a complete gravitational-settling calculation. Furthermore, as pre–white-dwarf evolution is uncertain, the assumption that the subsurface layer of a DA star is composed of helium cannot be verified. Thus the present hypothesis should be exploratory rather than definitive.

XIV. SUMMARY

Model-atmosphere calculations have been used to derive the masses and radii of white dwarfs. These results, which are presented in tables 4, 6, and 7, are in general agreement with gravitational redshifts and are consistent with the mass-radius relations for degenerate configurations. The data do not support the contention of Strittmatter and Wickramasinghe that there is a shortage of DA stars with $15{,}000° \leq T_{\rm eff} \leq 18{,}000°$ K. I have proposed a modification of their hypothesis which explains the existence of DB and DC stars in the appropriate temperature ranges.

I thank Dr. J. B. Oke for advice on all aspects of this thesis, and for the observing program which formed the basis of this work. I am extremely grateful to Dr. J. L. Greenstein for advice and encouragement. I thank Dr. J. E. Gunn for helpful conversations, and Dr. John Graham for permission to use unpublished material. Dr. V. Weidemann's comments on an earlier version of this manuscript have been extremely helpful. Computing time was generously supplied by the California Institute of Technology, and financial support by the National Science Foundation.

REFERENCES

Allen, C. W. 1963, *Astrophysical Quantities* (2d ed.; London: Athlone Press).
Altena, W. F. van. 1969, *A.J.*, **74**, 2.
———. 1971, *Ap. J.* (*Letters*), **165**, L177.
Angel, J. R. P. 1972, *Ap. J.* (*Letters*), **171**, L17.
Barnard, A. J., Cooper, J., and Shamey, L. J. 1969, *Astr. and Ap.*, **1**, 28.
Böhm, K.-H., and Stückl, E. 1967, *Zs. f. Ap.*, **66**, 487.
Bos, W. H. van den. 1960, *J. d'Obs.*, **43**, 145.
Bues, I. 1970, *Astr. and Ap.*, **7**, 91.
Chin, C.-W., and Stothers, R. 1971, *Ap. J.*, **163**, 555.
Danby, J. M. A., and Camm, R. 1957, *M.N.R.A.S.*, **117**, 50.
Demarque, P., and Mengel, J. 1971, *Ap. J.*, **164**, 469.
Edmonds, F. N., Schlüter, H., and Wells, D. C., III. 1967, *Mem. R.A.S.*, **71**, 271.
Eggen, O. J. 1969, *Ap. J.*, **157**, 287.
Eggen, O. J., and Greenstein, J. L. 1965*a*, *Ap. J.*, **141**, 83 (EG I).
———. 1965*b*, *ibid.*, **142**, 925 (EG II).
———. 1967, *ibid.*, **150**, 927 (EG III).
Gingerich, O. J., Latham, D. W., Linsky, J. L., and Kumar, S. S. 1966, in *Colloquium on Late-Type Stars*, ed. M. Hack (Trieste: Observatorio Astronomico di Trieste), p. 291.
Gliese, W. 1969, *Catalogue of Nearby Stars* (Heidelberg Pub. No. 22).
Goldberg, L., Müller, E. A., and Aller, L. H. 1960, *Ap. J. Suppl.*, **5**, 1 (GMA).
Graham, J. A. 1969, in *Proceedings of the Symposium on Low-Luminosity Stars*, ed. S. S. Kumar (New York: Gordon & Breach), p. 139.
———. 1972, *A.J.*, **77**, 144.
Greenstein, J. L. 1969*a*, *Ap. J.*, **158**, 281.
———. 1969*b*, *Comments Ap. and Space Phys.*, **1**, 62.
———. 1970, *Ap. J.* (*Letters*), **162**, L55.
Greenstein, J. L., Oke, J. B., and Shipman, H. L. 1971, *Ap. J.*, **169**, 563.
Greenstein, J. L., and Trimble, V. 1967, *Ap. J.*, **149**, 283 (GT).
Griem, H. R. 1964, *Plasma Spectroscopy* (New York: McGraw-Hill Book Co.).
———. 1968, *Ap. J.*, **154**, 1111.
Hamada, T., and Salpeter, E. E. 1961, *Ap. J.*, **134**, 683.

Harman, R. J., and Seaton, M. J. 1964, *Ap. J.*, **140**, 824.
Hubbard, W. B., and Wagner, R. L. 1970, *Ap. J.*, **159**, 93.
Jenkins, L. F. 1963, *General Catalogue of Trigonometric Stellar Parallaxes* (New Haven: Yale University Observatory).
Kurucz, R. L. 1969*a*, *Ap. J.*, **156**, 235.
———. 1969*b*, in *Theory and Observation of Normal Stellar Atmospheres*, ed. O. Gingerich (Cambridge: MIT Press), p. 395.
Mathews, T. A., and Sandage, A. R. 1963, *Ap. J.*, **138**, 30.
Matsushima, S., and Terashita, Y. 1969*a*, *Ap. J.*, **156**, 183.
———. 1969*b*, *ibid.*, p. 219.
Oke, J. B. 1969, *Pub. A.S.P.*, **81**, 11.
———. 1972 (in preparation).
Oke, J. B., and Schild, R. E. 1970, *Ap. J.*, **161**, 1015.
Ostriker, J. P., and Bodenheimer, P. 1968, *Ap. J.*, **151**, 1089.
Peterson, V. 1969, thesis, California Institute of Technology.
Popper, D. M. 1954, *Ap. J.*, **120**, 316.
Riddle, R. K. 1970, *Pub. U.S. Naval Obs.*, Vol. **20**.
Shipman, H. L. 1971*a*, thesis, California Institute of Technology.
———. 1971*b*, *Ap. J.*, **166**, 587.
Strittmatter, P. A., and Wickramasinghe, D. T. 1971, *M.N.R.A.S.*, **152**, 47 (SW).
Terashita, Y., and Matsushima, S. 1969, *Ap. J.*, **156**, 203.
Trimble, V. L., and Greenstein, J. L. 1972, *Ap. J.* (submitted).
Van Horn, H. M. 1968, *Ap. J.*, **151**, 227.
Wagman, N. E. 1965, *A.J.*, **70**, 581.
———. 1967, *ibid.*, **72**, 957.
Wayman, P. A., Symms, L. S. T., and Blackwell, K. C. 1965, *R.O.B.*, No. 98.
Wegner, G. V. 1971, *Proc. Astr. Soc. Australia*, **2**, 30.
Weidemann, V., 1963, *Zs. f. Ap.*, **57**, 87.
———. 1968, *Ann. Rev. Astr. and Ap.*, **6**, 351.
Wiese, W. L., and Kelleher, D. E. 1971, *Ap. J.* (*Letters*), **166**, L59.
Wickramasinghe, D. T., and Strittmatter, P. A. 1971, *M.N.R.A.S.*, **150**, 435.
Wright, K. O., Lee, E. K., Jacobson, T. L., and Greenstein, J. L. 1964, *Pub. Dom. Ap. Obs.*, **12**, 173.